

RSC Advances



This is an *Accepted Manuscript*, which has been through the Royal Society of Chemistry peer review process and has been accepted for publication.

Accepted Manuscripts are published online shortly after acceptance, before technical editing, formatting and proof reading. Using this free service, authors can make their results available to the community, in citable form, before we publish the edited article. This *Accepted Manuscript* will be replaced by the edited, formatted and paginated article as soon as this is available.

You can find more information about *Accepted Manuscripts* in the [Information for Authors](#).

Please note that technical editing may introduce minor changes to the text and/or graphics, which may alter content. The journal's standard [Terms & Conditions](#) and the [Ethical guidelines](#) still apply. In no event shall the Royal Society of Chemistry be held responsible for any errors or omissions in this *Accepted Manuscript* or any consequences arising from the use of any information it contains.

Effect of HfO₂ on the Compatibility of Borosilicate Sealing Glasses for Solid Oxide Fuel Cells Application

Honglin Liu, Dandan Zhao, Shunrun Chen, Jinwan Huang, Dian Tang and Teng Zhang*

College of Materials Science and Engineering, Fuzhou University, Fuzhou, Fujian, 350108, China.

The interfacial reaction between sealing glasses and Cr-containing interconnects presents a challenge for the development of Solid Oxide Fuel Cells (SOFCs). In this paper, attention was focused on the relationship between the glass structure of HfO₂-containing borosilicate glasses and interfacial reaction between glasses and Crofer 22 APU. The results show that HfO₂ dissolves in the glass network with the form of Q² species and condenses the glass structure of borosilicate glasses. In addition, the fraction of Cr⁶⁺ in reaction couples between Cr₂O₃ and glass powders decreases with increasing HfO₂ content from 2 to 8 mol%. Moreover, the thickness of reaction zone is about 1 μm for glass with 2 mol% HfO₂/Crofer 22 APU, while no obvious reaction zone can be observed in glass with 8 mol% HfO₂/Crofer 22 APU. The reported results support the suitability of the prepared glass-ceramics as sealing materials for SOFCs applications.

Key Words: Solid Oxide Fuel Cells; Sealing Glass; Glass Structure; Interfacial Reaction; Hafnia

* Corresponding author. Tel.: +86 591 22866540; fax: +86 591 22866537.

E-mail address: teng_zhang@fzu.edu.cn (T. Zhang).

1. Introduction

In spite of the rapid progress on the Solid Oxide Fuel Cells (SOFCs) technology in last decade,^{1,2} the long term stability of SOFCs stack still remains a challenge. For example, the thermal stress in the stack often induces the generation and propagation of cracks at the interfaces and subsequently leads to the failure of stack upon frequent thermal cycles.^{3,4} Majumdar *et al.* reported that the main reasons for the generation of thermal stress include the installation process, the coefficient of thermal expansion (CTE) mismatch between different SOFCs components as well as the thermal gradient within the stack.⁵

Many efforts have been focused on the development of resilient seals (or resilient glasses) in recent years.⁶⁻⁹ Ideally the glass should remain viscous at high temperature, *i.e.*, 700-800 °C, to release the thermal stress generated by any CTE mismatch during thermal cycles. The glass melt should also flow to heal any cracks in the seals that form during operation, and still maintain the necessary mechanical strength to support the substrates. Lu *et al.* developed a SrO-La₂O₃-Al₂O₃-B₂O₃-SiO₂ glass system, which remains in amorphous state upon heating at 700 °C for 1500 hours.¹⁰ Reddy *et al.* also reported that the addition of ZrO₂ decreases the devitrification tendency of the CaO-MgO-SrO-Al₂O₃-La₂O₃-SiO₂-B₂O₃-Bi₂O₃ glass system, and thus leads to a glass does not crystallize after heating at 800 °C for 500 hours.¹¹

However, the detrimental interfacial reaction between Cr-containing interconnects and sealing glasses have been extensively reported in literature. Ogasawara *et al.* reported that the reaction between alkali components in sealing glasses and ZMG232 alloys leads to the formation of Na₂CrO₄(g) and K₂CrO₄, which often deposit on the surface of cathode and subsequently cause the degradation of

cathode.¹² In addition, the formation of BaCrO₄ (or SrCrO₄)^{13,14} is well known to be responsible for the physical separation between sealing glass and metallic interconnect,^{15,16} due to its much higher coefficient of thermal expansion (CTE) compared with glass and interconnect ($18-20 \times 10^{-6} \text{ K}^{-1}$ vs. $10-13 \times 10^{-6} \text{ K}^{-1}$).^{1,14} Moreover, our recent work also reveals that the alkaline earth ions (Sr²⁺) in glass matrix is much easier to react with Cr-containing interconnect to form the detrimental chromate phase, *e.g.*, SrCrO₄, compared with its analogue in crystalline phases.¹⁷ Therefore, the chemical compatibility presents a challenge for the development of sealing glasses, especially for resilient glasses.

On the other hand, it has been found that the glass transition temperature increases with increasing HfO₂ content in alumino-borosilicate glasses,¹⁸ indicating the densification of glass network and the decrease in devitrification tendency.¹⁹ The interfacial reaction, between HfO₂-doped borosilicate glasses and Cr-containing interconnects, thus provides a good modeling system to investigate the effect of glass structure on the interfacial reaction, without the interference of crystallization process. In addition, HfO₂ is well known as a high-K gate dielectric,^{20,21} which might be helpful for fulfilling the insulating requirement of sealing glasses. To the best of our knowledge, there are no reports on the interfacial reaction between HfO₂-containing sealing glasses and Cr-containing interconnect.

In this paper, HfO₂ was added gradually, from 2 to 8 mol%, to a representative Sr-containing borosilicate sealing glass. Attention was focused on the following questions: (1) How does HfO₂ affect the structures of glasses and glass-ceramics? (2) How does HfO₂ affect the thermal and electrical properties of glasses? (3) How does HfO₂ affect the interfacial reaction between sealing glasses and Cr-containing interconnects?

2. Experimental

2.1 Preparation of glass

A 50-g sample of each glass was prepared by melting a homogeneous mixture of reagent grade alkaline earth carbonates, boric acid, and various oxides (Sinopharm Chemical Reagent Co., Ltd.) in a platinum crucible in air at 1500 °C for one hour. The nominal compositions of glasses (mol%) are shown in Table 1. The ratios of B to Si and (Ca+Sr) to Si were kept constant to clarify the effect of Hf/Si ratio on the structure and properties of sealing glasses. Some of the melt was poured into stainless steel mold to obtain cylindrical shaped glass specimens (25 mm length and 10 mm diameter for CTE measurement, 5 mm length and 10 mm diameter for resistance test.) and the rest of the melt was quenched on a steel plate. Glass powders were then crushed and sieved to a particle size of 45 to 53 μm (manual sieve, 270 and 325 meshes, Sinopharm Chemical Reagent Co., Ltd.).

2.2 Characterization of glass structure and crystalline structure of glass-ceramics

The FTIR absorption spectra of quenched glasses were recorded at room temperature in the range 400-1600 cm^{-1} using FTIR spectrometer (Nicolet 5700, Thermo scientific Inc.) with a spectral resolution of 2 cm^{-1} . A KBr pellets technique was used for preparing the samples.

Raman spectra of quenched glass powders were collected in 400-1600 cm^{-1} wave number range by Raman spectrometer (Renishaw invia). The light source was 514.5 nm argon laser with 400 seconds of exposure time. The spectra were analyzed by Gaussian fitting with the Origin 8.0 software.

NMR ^{29}Si , magic angle spinning (MAS) nuclear magnetic resonance (NMR) spectra were recorded for all quenched glasses. The spectra were acquired on a Bruker

AVANCE III 600 spectrometer operating at a field of 9.4 T with ^{29}Si Larmor frequencies of 119.2 MHz.

The O1s XPS spectra of quenched glasses were obtained by X-ray photoelectron spectroscopy (ESCALAB 250, Thermo Scientific, Inc.) using a monochromatic Al K α source (10 mA, 15 kV). The spectra were analyzed using the Thermo Avantage software.

The crystalline phases in glass-ceramic powders, after holding at 800 °C for 100 hours, were identified by X-ray diffraction (XDS 2000, Scintag, Inc.).

2.3 Characterization of thermal and electrical properties of glass

The glass transition temperature (T_g) and the onset crystallization temperature (T_c) of glass powders were determined using differential scanning calorimetry (SDTQ600, TA, Inc.) at a heating rate of 10 °C·min $^{-1}$.

The thermal characteristics of the quenched glasses, including the CTE (between 200 and 600 °C), glass transition temperature (T_g), and softening temperature (T_d), were determined by a dilatometer (DIL402C, NETZSCH, Inc.) at 10 °C·min $^{-1}$ in air.

The conductivity of glass cylinders using dense disk-shaped samples with Pt current collectors and Pt wire, in air from 600 to 700 °C at a heating rate of 5 °C·min $^{-1}$, was measured using a high resistance meter (4339B, Agilent, Inc.).

2.4 Characterization of interfacial reaction

It is well established that alkaline earth oxides (*e.g.*, BaO or SrO) in the sealing glasses often react with Cr-containing interconnects in air and form chromate phases such as BaCrO $_4$ or SrCrO $_4$.^{16,22-24} Our previous work also found that the reaction between SrO-containing glasses and Cr $_2$ O $_3$ results in the formation of SrCrO $_4$.^{25,26} In addition, SrCrO $_4$ has been identified at the interface between sealing glass and Crofer 22 APU.²⁶ Moreover, we have measured the UV adsorption of the solution containing

unreacted Cr_2O_3 held in air at 950 °C for 24 hours, and did not detect any signals of Cr^{6+} .²⁶ This confirms that the Cr^{6+} only comes from the reaction product, *i.e.* SrCrO_4 .

A ~10 mg mixture of glass and 10 wt% Cr_2O_3 powders was reacted in an alumina boat in air for different time. The reaction temperature was set to be 700 °C to exclude the effects of crystallization and softening processes. The reaction product was dissolved into ~50 ml of NaOH solution (PH=10~12) and the absorption spectra were recorded using the UV-VIS Spectrometer (Optima 2000 DV, Perkin Elmer, Inc.). The fraction of Cr^{6+} was then calculated by fitting the measured absorption to the calibration curve. The detailed procedure of this quantitative analysis has been discussed elsewhere.^{25,26}

Glass pastes were prepared by mixing ~50 mg glass powder (45-53 μm) with ~50 μl acetone. The pastes were applied to the ultrasonically-cleaned surfaces of Crofer 22 APU. The coated samples were then held in air at 800 °C for 1000 hours. The glass/metal sealing couples were polished using SiC paper from 320 to 1200 grit, and then finished using an alumina suspension (3 μm). The polished samples were analyzed using field emission scanning electron microscopy (Supra-55, Zeiss, Inc.) and X-ray energy dispersive analysis (EDS, X-Max, OXFORD instruments, Inc.).

3. Results and discussion

3.1 Glass structure

It is known that deconvolution has been widely used for resolving band-overlapping problems,²⁷ especially for the Raman and FT-IR spectra.^{28,29} For simplicity, the absorption FTIR spectra of glasses containing 2 and 8 mol% HfO_2 (H2 and H8) have been deconvoluted, as shown in Fig.1. The peak located at about 500 cm^{-1} relates to the overlapping bending modes of the Si-O-Si and B-O-B.^{30,31} The 729 cm^{-1} peak can be attributed to the Si-O-B bending vibrations.³¹ The peak at 802 cm^{-1}

might have contributions from Si-O-Hf and Si-O-Si group.³² Considering the increasing intensity of the 804 cm^{-1} peak with greater HfO_2 content in glasses, one can readily assign this peak to Si-O-Hf group in this work.

The peaks in the range of 800-1200 cm^{-1} , including 850, 929, 1012, 1086, and 1186 cm^{-1} , are due to the stretching vibration of $[\text{BO}_4]$ tetrahedron units in various structural groups.³³⁻³⁶ In addition, the 1200-1600 cm^{-1} peaks, including 1250, 1384, 1450 and 1507 cm^{-1} , can be assigned for the stretching vibrations of $[\text{BO}_3]$ units.³³ Based on the integrated areas of peaks for $[\text{BO}_3]$ and $[\text{BO}_4]$ units, one can calculate that the ratio of $[\text{BO}_4]$ to $[\text{BO}_3]$ units decreases from 3.1 to 2.5 when HfO_2 content increases from 2 to 8 mol%. This indicates that the addition of HfO_2 induces the conversion of $[\text{BO}_4]$ to $[\text{BO}_3]$. Bergaeron *et al.* also reported that the addition of IVB elements in soda-lime borosilicate glasses leads to a decreasing proportion of $[\text{BO}_4]$, due to competition for charge compensation between B and Zr, Hf or Ti.³⁷

Fig.2 shows the deconvoluted Raman spectra of quenched glasses with different HfO_2 contents. In the wave number region of 400-800 cm^{-1} , the spectra contain both B-O-B and Si-O-Si bonds.³⁸ The 650 cm^{-1} peak indicates the presence of pentaborate and dipentaborate structural units.³⁹ It has been reported that the 703 cm^{-1} peak in $\text{ZrO}_2\text{-Na}_2\text{O-Li}_2\text{O-B}_2\text{O}_3\text{-SiO}_2$ glass is due to the tentative Zr-O stretch.⁴⁰ Considering the similarity between Zr-O and Hf-O,³⁷ the peak centered at about 705 cm^{-1} can be ascribed to Hf-O bond.

In addition, the spectra in the range of 800-1200 cm^{-1} are often used for quantitative analysis of different $[\text{SiO}_4]$ structural units, *i.e.*, Q^n ($n=0, 1, 2, 3$ and 4 , where n is the number of connecting bonds in $[\text{SiO}_4]$ tetrahedral unit).^{41,42} It is worth noting that the Q^2 content increases from 42 % for H2 to 59 % for H8. McKeown *et al.* investigated the structural change of ZrO_2 -doped borosilicate glasses using Raman

spectroscopy.⁴⁰ They found that as zirconia content in the glass is increased, the band assigned to Si-O stretch in Q² units (silicate chains) increases in area, while band areas decrease for modes assigned to Si-O stretch in more polymerized Q³ and Q⁴ units (silicate sheets and cages). Bihuniak *et al.* also observed similar Raman spectra in zirconium and hafnium-containing vitreous silicas and concluded that each metal atom (zirconium and hafnium) bonded to two oxygen atoms of a [SiO₄] unit (*i.e.*, Q²).⁴³ Moreover, the previous studies on the effect of ZrO₂ on the structure of borosilicate glass⁴⁰ and lithium silicate glass¹⁹ revealed that the Zr⁴⁺ ions prefer to enter in Q² species rather than in Q³ and Q⁴. Considering the similar effects of Zr and Hf on the structure of borosilicate glasses,³⁷ one can deduce that Q² units increases with increasing HfO₂ content.

Shown in Table 2 is the Qⁿ distribution of sealing glasses. Based on the Qⁿ distribution, one can found that Q⁰ decreases from 30% to 18% as HfO₂ content increases from 2 to 8 mol%, in addition to the decrease in Q³ and Q⁴. This indicates that Q² increases as HfO₂ content increases, at the expense of Q⁰, Q³ and Q⁴.

To clarify the effect of HfO₂ on the silicate structure, we have also calculated the ratio of bridging oxygen (BO) to non-bridging (NBO) based on Raman results. The ratio of BO/NBO increases from 0.60 to 0.63, indicating that the overall silicate structure strengthens as HfO₂ content increases.

Between 1200 and 1600 cm⁻¹, the peaks are associated with stretching of B-O bonds attached to large borate groups.⁴⁴ The peaks at about 1410 cm⁻¹ is due to BO₃ triangles linked to BO₄ units; whereas, the peaks at about 1490 cm⁻¹ can be assigned to BO₃ triangles linked to other BO₃ units.^{44,45} Based on the integrated areas of these two peaks ($A_{[BO_3]}$ for 1490 cm⁻¹ peak and $A_{[BO_4]}$ for 1410 cm⁻¹ peak), one can calculate that $A_{[BO_4]}/A_{[BO_3]}$ decrease from 1.2 to 0.4 with the increase in HfO₂ content

from 2 to 8 mol%. This also indicates the conversion of [BO₄] to [BO₃] in glasses with HfO₂ dopant, consistent with the FTIR results (in Fig.1).

Fig.3 shows the ²⁹Si MAS NMR spectra of the glasses. The peaks near -80 and -100 ppm can be assigned to Q² and Q⁴, respectively.⁴⁶ The chemical shift of ²⁹Si from -79 for H2 to -82 ppm for H8 indicates an increasing densification degree of [SiO₄] tetrahedral with increasing HfO₂ content.¹¹ Three peaks present at about -80, -90 and -110 ppm in the deconvoluted NMR spectra, corresponding for Q², Q³ and Q⁴, respectively.⁴⁶ It is clear that Q² increases with increasing HfO₂ content, which is in good agreement with the Raman results (in Fig.2).

In addition, the O1s XPS curves are often deconvoluted into two peaks, *i.e.*, BO and NBO. The fraction of BO can be calculated by comparing the integrated areas of two peaks and thus provides quantitative information on the overall glass structure. Fig.4 shows the deconvoluted O1s spectra of quenched glasses with different HfO₂ contents. The fraction of BO in glasses increases from 78% for H2 to 87% for H8. This denotes that the presence of HfO₂ leads to the densification of glass structure.

3.2 Thermal and electrical properties

Shown in Table 3 are the thermal properties of quenched glasses. The glass transition temperature (T_g) of quenched glasses, measured by DSC, increases from 682 °C for H2 to 690 °C for H4 and to 712 °C for H8. The onset crystallization temperature (T_c) of glasses also increases from 818 °C for H2 to 832 °C for H4 and to 879 °C for H8. The temperature difference between T_g and T_c, ΔT = T_c-T_g, is generally taken for evaluating the glass forming ability (GFA) of glasses.⁴⁷ The ΔT of glasses increases from 136 to 167 °C when the HfO₂ content increases from 2 to 8 mol% (in Table 3), which implies that the glass forming ability of quenched glasses is improved with the addition of HfO₂.

In addition, the glass transition temperature (T_g) of quenched glasses, measured by dilatometer, increases from 680 ± 3 °C for H2 to 735 ± 3 °C for H8. The softening temperature (T_d) also increases from 738 ± 3 °C for H2 to 800 ± 3 °C for H8 (in Table 3). The increase in glass transition temperature and softening temperature further verifies the densification of glass network with HfO₂ dopant.

On the other hand, the CTE of quenched glasses decreases from 11.5 ± 0.1 for H2 to $10.7 \pm 0.1 \times 10^{-6}$ K⁻¹ for H8. The decrease in CTE with HfO₂ dopant again verifies the densification of glass network. It is also worth noting that the CTEs of HfO₂-doped glasses fall in the design range of sealing glasses ($9.5\text{-}12.0 \times 10^{-6}$ K⁻¹).⁴⁸

Fig.5 shows the temperature dependence of conductivity ($\log \sigma$ versus $1000/T$) for glasses, measured in air from 600 to 700 °C. The conductivity (σ) of all species increases with increasing temperature. In addition, the conductivity of quenched glasses at each temperature decreases with HfO₂ dopant. For example, the conductivity (σ) of glasses at 700 °C decreases from 4.0×10^{-7} S·cm⁻¹ for H0 to 1.1×10^{-7} S·cm⁻¹ for H8. Karlsson *et al.* reported that the replacement of Ca by Na in the Na₂O-CaO-SrO-SiO₂ glasses opens up the structure and allows the formation of diffusion pathways, thus enhancing the diffusion of both Na and Ca.⁴⁹ Thus, the decrease in conductivity of glasses with increasing HfO₂ content in this work can be attributed to the densification of glass network by HfO₂ dopant. It is also worth noting that the conductivity of HfO₂-containing glasses at 700 °C ranges from 1.1×10^{-7} S·cm⁻¹ to 2.6×10^{-7} S·cm⁻¹, meeting the insulating requirement of sealing glasses ($<10^{-4}$ S·cm⁻¹) for SOFCs application.⁵⁰

Fig.6 shows the XRD patterns of glasses held at 800 °C for 100 hours. The main phases in H2 include Sr₃Si₃O₉ (ICDD Card No.75-2281) and Ca₆Hf₁₉O₄₄ (ICDD Card

No.36-0524); whereas, a new Hf-containing phase, *i.e.*, $\text{Ca}_3\text{HfSi}_2\text{O}_9$ (ICDD Card No.83-0364), becomes significant with increasing HfO_2 content in glasses.

3.3 Interfacial reaction

It is well established that the nature of the interfacial reaction between sealing glass and metallic interconnect is the reaction between sealing glass and the Cr_2O_3 layer formed on the surface of interconnect under the routine operation of SOFC.^{22,26} Therefore, we mixed with Cr_2O_3 and tested the reaction between Cr_2O_3 and glass to simulate the interfacial reaction between Cr-containing interconnects and glass, which has been proved to be appropriate by many previous works in literature.^{17,25,26} Shown in Fig.7 is the fraction of Cr^{6+} in the reaction couples between Cr_2O_3 and glass powders, after reacting in air at 700 °C, as a function of reaction time. It is worth noting that the fraction of Cr^{6+} in the reaction couples decreases with increasing HfO_2 content. Our recent work on the chemical compatibility of borosilicate glasses revealed that the fraction of Cr^{6+} in the glass/ Cr_2O_3 reaction couples at 700 °C decreases when Al_2O_3 content increases from 2 to 8 mol%, due to the densification of glass network.⁵¹ Therefore, the improvement in chemical compatibility of glasses can also be attributed to the densification of glass network with the addition of HfO_2 .

Fig.8 shows the images of glass-metal interfaces held at 800 °C for 100 hours, along with the elemental EDS line scans taken across the interface. The results of EDS elemental analysis at selected points in the glass-ceramics are summarized in Table 4. It is clear that a good joining can be observed at the interfaces between Crofer 22 APU and glasses with HfO_2 dopant. In addition, the Hf enrichment is observed in the white regions of the glass-ceramics, *e.g.*, points#1, #4 and #5. This implies that Hf has been incorporated into the crystalline phase, consistent with the observed Hf-containing phases in the XRD patterns (in Fig.6).

However, the EDS line scan reveals that the thickness of reaction zone (enrichment in Sr, Cr, Mn and O) is about 1 μm for H2/Crofer 22 APU, while no obvious reaction zone can be observed in H8/Crofer 22 APU. In addition, considerable amounts of Sr, Cr, Mn and Fe can be detected in the interdiffusion zone between H2 and Crofer 22 APU (point#3 in Fig.8a); whereas, the Cr content at the H8/Crofer 22 APU interface is only about 2 at% (point#6 in Fig.8a). It is also worth noting that the Hf contents in point#3 and point#6 are 0 and 4 at%, respectively. These experiential results further support the positive effect of HfO₂ on the reduction of detrimental interfacial reaction between glass and metallic interconnect (in Fig.7). It is known that the diffusion of a given mobile ion in glasses depends on temperature as well as the glass structure.^{52,53} The addition of HfO₂ leads to the densification of glass structure, which decreases the interdiffusion between sealing glasses and Crofer 22 APU, and consequently reduces the detrimental interfacial reaction in this work.

4. Conclusions

The effect of glass structure on the interfacial reaction between HfO₂-doped glasses and Cr-containing interconnect was clearly demonstrated in present work. The addition of HfO₂ strengthens the glass structure, increases the glass forming ability and decreases the conductivity of sealing glasses. In addition, the condensed glass structure blocks the interdiffusion between glasses and Crofer 22 APU, and thus reduces the detrimental interfacial reaction. The findings on the reduced glass/metal interfacial reaction by HfO₂ dopant will shed lights onto the development of stable glasses for SOFCs application.

Acknowledgments

The authors gratefully acknowledge the financial support of the National Natural Science Foundation of China (No. 51102045), Program for New Century Excellent Talents in Fujian Province University (No. JA12013) and the National Undergraduate Innovative Experiment Program (No. 201410386031). They would also like to thank Qidi Chen for assistance with SEM/EDS, Zhenhuan Zheng for assistance with X-ray diffraction and Fen Lin for assistance with DSC and dilatometric analyses.

References

1. D. U. Tulyaganov, A. A. Reddy, V. V. Kharton, J. M. F. Ferreira, *Journal of Power Sources*, 2013, **242**, 486-502.
2. Y.-S. Chou, J. W. Stevenson, J.-P. Choi, *Journal of Power Sources*, 2014, **250**, 166-173.
3. F. Smeacetto, A. Chrysanthou, T. Moskalewicz M. Salvo, *Materials Letters*, 2013, **111**, 143-146.
4. Y.-S. Chou, E. C. Thomsen, J. P. Choi, J. W. Stevenson, *Journal of Power Sources*, 2012, **197**, 154-160.
5. S. Majumdar, T. Claar, B. Flandermeyer, *Journal of the American Ceramic Society*, 1986, **69**, 628-633.
6. F. Smeacetto, M. Salvo, M. Ferraris, V. Casalegno, P. Asinari, A. Chrysanthou, *Journal of the European Ceramic Society*, 2008, **28**, 2521-2527.
7. A. Goel, D. U. Tulyaganov, V. V. Kharton, A. A. Yaremchenko, J. M. F. Ferreira, *Journal of Power Sources*, 2010, **195**, 522-526.
8. T. Moskalewicz, F. Smeacetto, G. Cempura, L. C. Ajitdoss, M. Salvo, A. Czyska-Filemonowicz, *Surface and Coatings Technology*, 2010, 204, 3509-3516.
9. A. A. Reddy, D. U. Tulyaganov, A. Goel, M. J. Pascual, V. V. Kharton, E. V. Tsipis, J. M. F. Ferreira, *International Journal of Hydrogen Energy*, 2012, **37**, 12528-12539.

10. K. Lu and W. Li, *Journal of Power Sources*, 2014, **245**, 752-757.
11. A. A. Reddy, D. U. Tulyaganov, A. Goel, M. Sardo, P. V. Wiper, M. J. Pascual, V. V. Kharton, V. A. Kolotygin, E. V. Tsipis, L. Mafra, J. M. F. Ferreira, *Journal of Materials Chemistry A*, 2013, **1**, 6471-6480.
12. F. Smeacetto, M. Salvo, M. Santarelli, P. Leone, G. A. Ortigoza-Villalba, A. Lanzini, L. C. Ajitdoss, M. Ferraris, *International Journal of Hydrogen Energy*, 2013, **38**, 588-596.
13. M. J. Pascual, A. Guillet, A. Durán, *Journal of Power Sources*, 2007, **169**, 40-46.
14. Y.-S. Chou, J. W. Stevenson, P. Singh, *Journal of Power Sources*, 2008, **184**, 238-244 .
15. F. Smeacetto, M. Salvo, M. Ferraris, V. Casalegno, P. Asinari, *Journal of the European Ceramic Society*, 2008, **28**, 611-616.
16. Z. Yang, J. W. Stevenson, K. D. Meinhardt, *Solid State Ionics*, 2003, **160**, 213-225.
17. T. Zhang, Q. Zou, F. Zeng, S. Wang, D. Tang, H. Yang, *Journal of Power Sources*, 2012, **216**, 1-4.
18. Y. Zhang, A. Navrotsky, H. Li, L. Li, L. L. Davis, D. M. Strachan, *Journal of Non-Crystalline Solids*, 2001, **296**, 93-101.
19. C.-C. Lin, P. Shen, H. M. Chang, Y. J. Yang, *Journal of the European Ceramic Society*, 2006, **26**, 3613-3620.
20. E. Verrelli, D. Tsoukalas, *Microelectronic Engineering*, 2011, **88**, 1189-1193.
21. M. A. Khaskheli, P. Wu, R. Chand, X. Li, H. Wang, S. Zhang, S. Chen, Y. Pei, *Applied Surface Science*, 2013, **266**, 355-359.
22. Y.-S. Chou, J. W. Stevenson, R. N. Gow, *Journal of Power Sources*, 2007, **170**, 395-400.
23. T. Jin, K. Lu, *Journal of Power Sources*, 2010, **195**, 4853-4864.
24. Z. Yang, G. Xia, K. Meinhardt, K. S. Weil, J. Stevenson, *Journal of Materials Engineering and Performance*, 2004, **13**, 327-334.
25. T. Zhang, H. Zhang, G. Li, H. Yung, *Journal of Power Sources*, 2010, **195**, 6795-6797.
26. T. Zhang, R. K. Brow, W. G. Fahrenholtz, S. T. Reis, *Journal of Power Sources*, 2012, **205**, 301-306.

27. H. Liu, L. Yan, Y. Chang, H. Fang, T. Zhang, *IEEE Transactions on Instrumentation and Measurement*, 2013, **62**, 315-327.
28. X. Zhu, C. Mai, M. Li, *Journal of Non-Crystalline Solids*, 2014, **388**, 55-61.
29. H. Fan, L. Hu, K. Yang, Y. Fang, *Journal of Non-Crystalline Solids*, 2010, **356**, 1814-1818.
30. E. Mansour, *Journal of Non-Crystalline Solids*, 2012, **358**, 454-460.
31. K. Annapurna, M. Das, P. Kundu, R. N. Dwivedi, S. Buddhudu, *Journal of Molecular Structure*, 2005, 741, 53-60.
32. L. Armelao, C. Eisenmenger-Sittner, M. Groenewolt, S. Gross, C. Sada, U. Schubert, E. Tondello, A. Zattin, *Journal of Materials Chemistry A*, 2005, **15**, 1838-1848.
33. Y. Cheng, H. Xiao, C. Shuguang, B. Tang, *Physica B: Condensed Matter*, 2009, **404** , 1230-1234.
34. Y. B. Saddeek, M. S. Gaafar, S. A. Bashier, *Journal of Non-Crystalline Solids*, 2010, **356**, 1089-1095.
35. R. Kaur, S. Singh, O. P. Pandey, *Physica B: Condensed Matter*, 2012, **407**, 4765-4769.
36. R. Kaur, S. Singh, O. P. Pandey, *Journal of Molecular Structure*, 2013, **1049**, 409-413.
37. B. Bergeron, L. Galoisy, P. Jollivet, F. Angeli, T. Charpentier, G. Calas, S. Gin, *Journal of Non-Crystalline Solids*, 2010, **356**, 2315-2322.
38. M. K. Mahapatra, K. Lu, R. J. Bodnar, *Applied Physics A*, 2009, **95**, 493-500.
39. R. Akagi, N. Ohtori, N. Umesaki, *Journal of Non-Crystalline Solids*, 2001, **293-295** , 471-476.
40. D. A. McKeown, I. S. Muller, A. C. Buechele, I. L. Pegg, C. A. Kendziora, *Journal of Non-Crystalline Solids*, 2000, **262**, 126-134. *Journal of Power Sources*, 2008, **185**, 993-1000.
42. B. G. Parkinson, D. Holland, M. E. Smith, C. Larson, J. Doerr, M. Affatigato, S. A. Feller, A. P. Howes, C. R. Scales, *Journal of Non-Crystalline Solids*, 2008, **354**, 1936-1942.
43. P. P. Bihuniak, R. A. Condrate, *Journal of Non-Crystalline Solids*, 1981, **44**, 331-343.
44. M. Lenoir, A. Grandjean, Y. Linard, B. Cochain, D. R. Neuville, *Chemical Geology*, 2008, **256**, 316-325.

45. D. Manara, A. Grandjean, D. R. Neuville, *American Mineralogist*, 2009, **94**, 777-784.
46. A. A. Reddy, D. U. Tulyaganov, G. C. Mather, M. J. Pascual, V. V. Kharton, S. I. Bredikhin, V. A. Kolotygin, J. M. F. Ferreira, *International Journal of Hydrogen Energy*, 2014, **39**, 3552-3563.
47. E. B. Ferreira, E. D. Zanotto, S. Feller, G. Lodden, J. Banerjee, T. Edwards, M. Affatigato, *Journal of the American Ceramic Society*, 2011, **94**, 3833-3841.
48. M. K. Mahapatra, K. Lu, *Materials Science & Engineering R-reports*, 2010, **67**, 65-85.
49. C. Karlsson, E. Zanghellini, J. Swenson, B. Roling, D. T. Bowron, L. Börjesson, *Physical Review B*, 2005, **72**, 064206.
50. P. Lessing, *Journal of Materials Science*, 2007, **42**, 3465-3476.
51. J. Chen, H. Yang, R. Chadeyron, D. Tang, T. Zhang, *Journal of the European Ceramic Society*, 2014, **34**, 1989-1996.
52. M. M. Smedskjaer, J. C. Mauro, S. Sen, J. Deubener, Y. Yue, *The Journal of Chemical Physics*, 2010, **133**, 154509.
53. D. K. McElfresh, D. G. Howitt, *Journal of Non-Crystalline Solids*, 1990, **124**, 174-180.

List of tables

Table 1 Batch composition (in mol%) of sealing glasses.

Table 2 Q^n distribution of sealing glasses with different HfO_2 contents.

Table 3 Thermal properties of sealing glasses with different HfO_2 contents.

Table 4 Compositions of selected spots in glass-ceramics determined by EDS (in at%).

Table 1 Batch composition (in mol%) of sealing glasses.

Sample ID	SrO	CaO	B ₂ O ₃	SiO ₂	HfO ₂
H2	25.5	25.5	7.8	39.2	2.0
H4	25.0	25.0	7.6	38.4	4.0
H6	24.4	24.4	7.5	37.7	6.0
H8	23.9	23.9	7.4	36.8	8.0

Table 2 Q^n distribution of sealing glasses with different HfO_2 contents.

Sample ID	Raman Data (%)					NMR Data (%)		
	Q ⁰	Q ¹	Q ²	Q ³	Q ⁴	Q ²	Q ³	Q ⁴
H2	30	15	37	11	7	78	14	8
H8	18	20	54	5	3	87	7	6

Table 3 Thermal properties of sealing glasses with different HfO₂ contents.

Sample ID	Hf0	H2	H4	H6	H8
Measured by DSC(°C)					
T _g	674 ± 3	682 ± 3	690 ± 3	702 ± 3	712 ± 3
T _c	823 ± 3	818 ± 3	832 ± 3	858 ± 3	879 ± 3
GFA=T _c -T _g	149	136	142	156	167
Measured by dilatometer(°C)					
T _d	739 ± 3	738 ± 3	761 ± 3	789 ± 3	800 ± 3
T _g	680 ± 3	692 ± 3	708 ± 3	726 ± 3	735 ± 3
CTE (× 10 ⁻⁶ K ⁻¹ , 200-600 °C)	11.5 ± 0.1	11.5 ± 0.1	11.1 ± 0.1	10.9 ± 0.1	10.7 ± 0.1

T_g: glass transition temperature

T_c: crystallization temperature

GFA: glass formation ability

T_d: softening temperature

CTE: coefficient of thermal expansion

Table 4 Compositions of selected spots in glass-ceramics determined by EDS (in at%).

points	Ca	Sr	Si	Hf	Cr	Mn	Fe
#1	18	32	21	29	0	0	0
#2	28	17	42	0	8	2	3
#3	6	7	11	0	40	26	10
#4	21	22	43	14	0	0	0
#5	9	35	17	36	2	1	0
#6	28	16	49	4	2	1	0

List of figures

Fig.1 Deconvoluted FTIR spectra of quenched glasses with different HfO₂ contents.

Fig.2 Deconvoluted Raman spectra of quenched glasses with different HfO₂ contents.

Fig.3 The ²⁹Si NMR spectra of quenched glasses with different HfO₂ contents.

Fig.4 Deconvoluted O1s spectra of quenched glasses with different HfO₂ contents.

Fig.5 The temperature dependence of conductivity (log σ versus 1000 T⁻¹), measured in air from 600 to 700 °C, for quenched glasses.

Fig.6 XRD patterns of glass-ceramics held at 800 °C for 100 hours.

Fig.7 The fraction of Cr⁶⁺ in the reaction couples between Cr₂O₃ and glass powders, after reacting in air at 700 °C, as a function of reaction time.

Fig.8 Micrographs of glass-ceramics/metal interfaces held at 800 °C for 100 hours, and EDS elemental line scans across the respective interfaces, for (a) glass containing 2 mol% HfO₂ and (b) glass containing 8 mol% HfO₂.

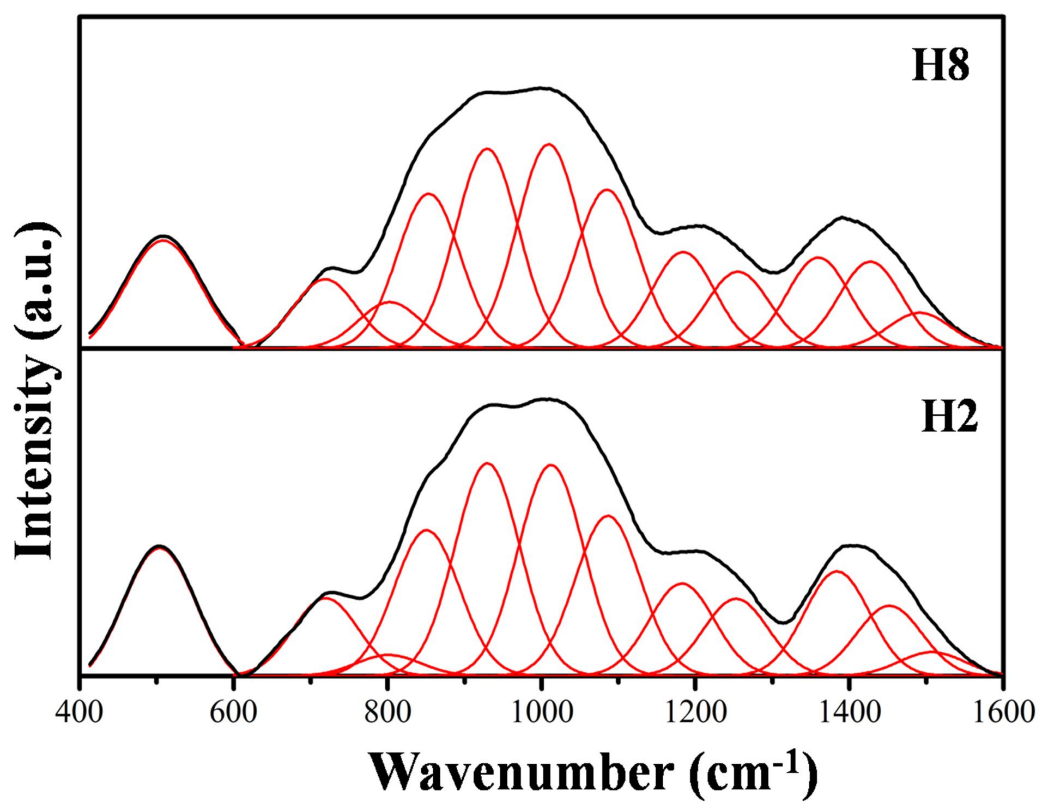


Fig.1 Deconvoluted FTIR spectra of quenched glasses with different HfO₂ contents.

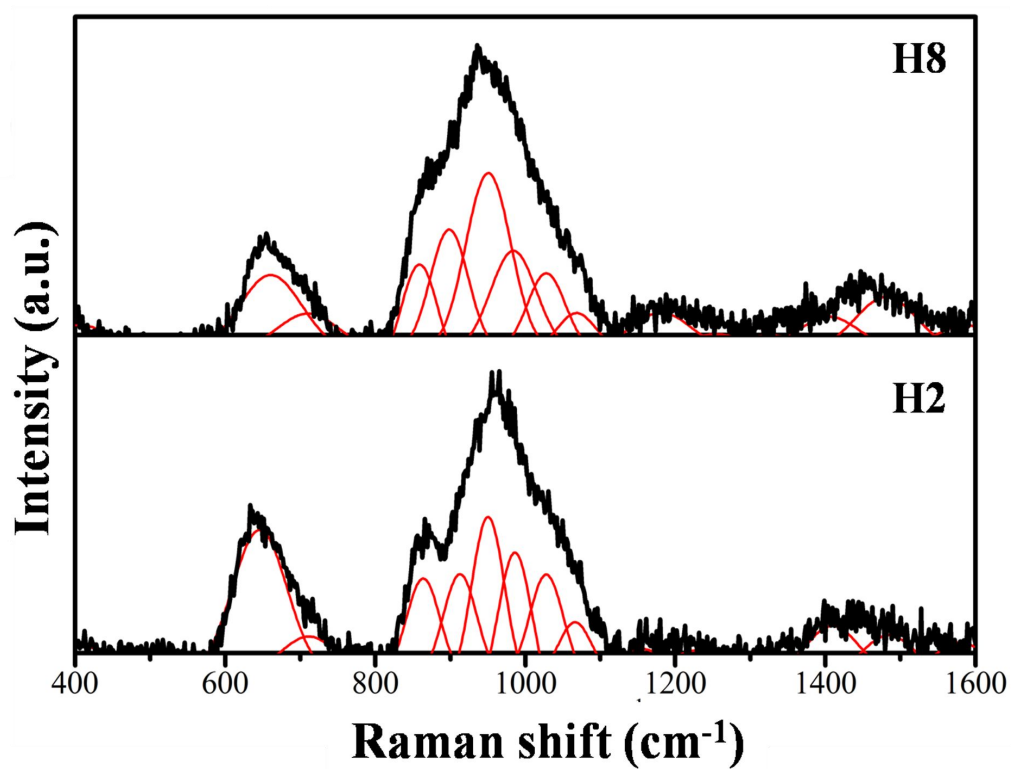


Fig.2 Deconvoluted Raman spectra of quenched glasses with different HfO₂ contents.

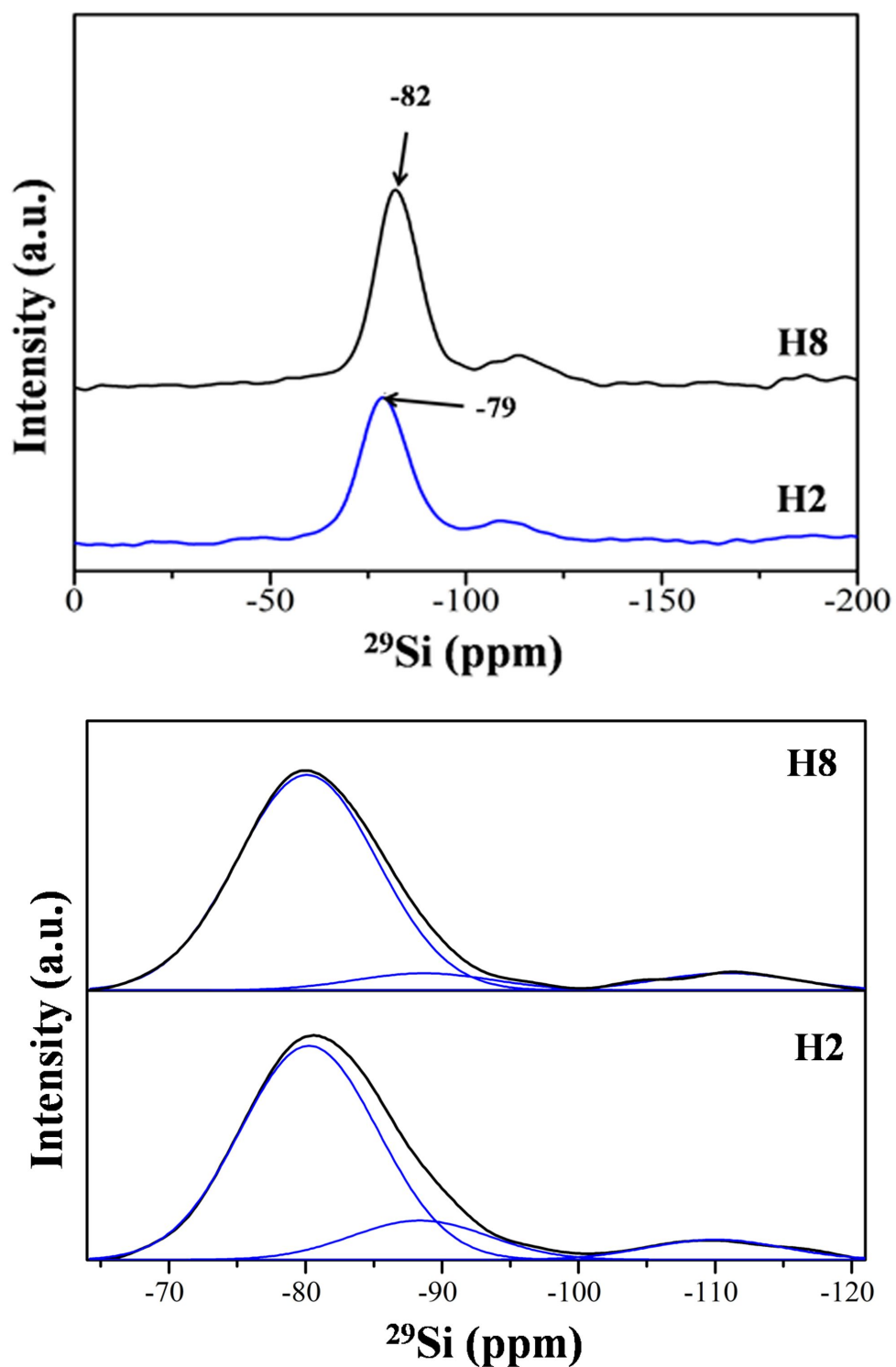


Fig.3 The ^{29}Si NMR spectra of quenched glasses with different HfO_2 contents.

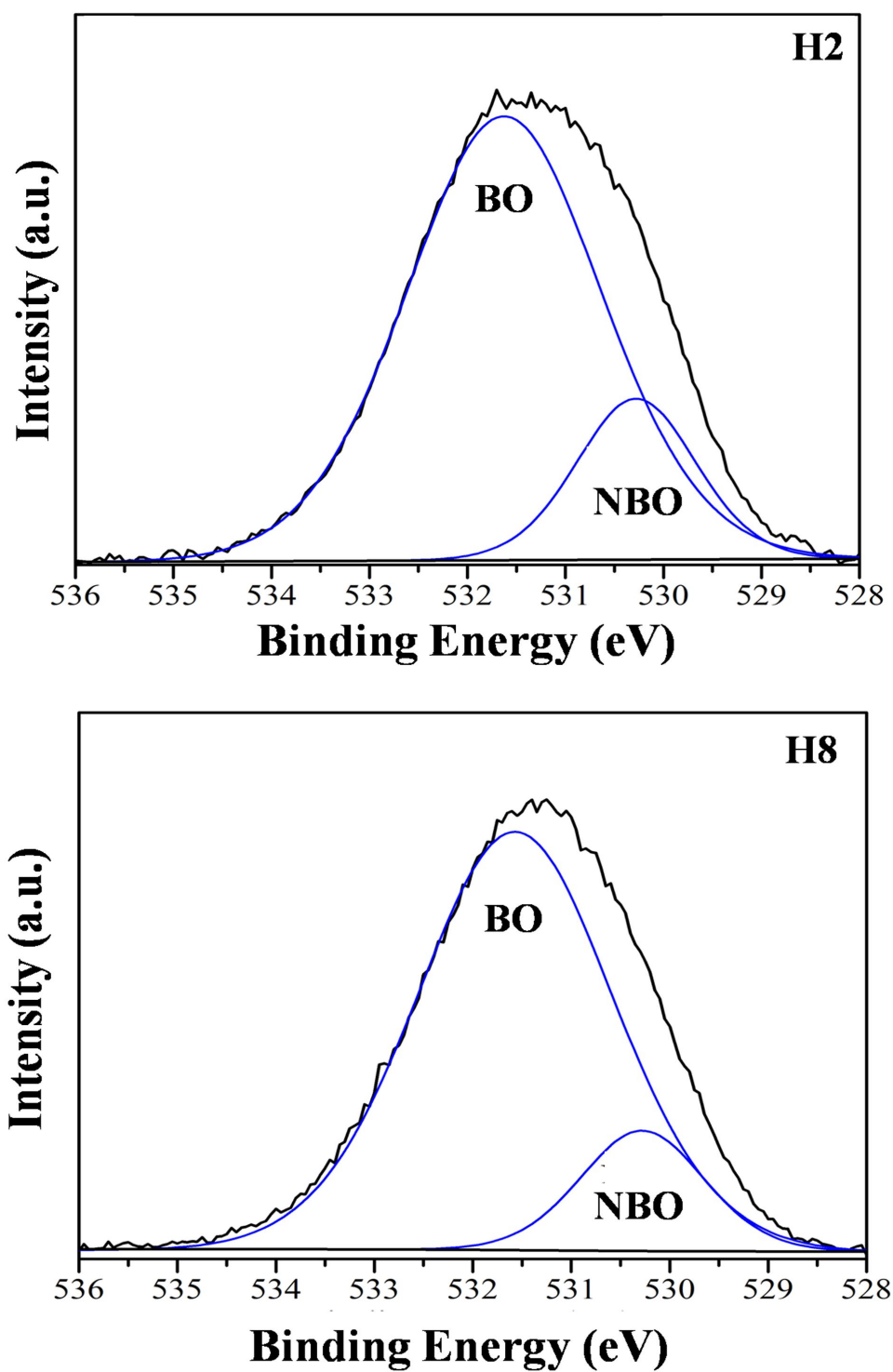


Fig.4 Deconvoluted O1s spectra of quenched glasses with different HfO₂ contents.

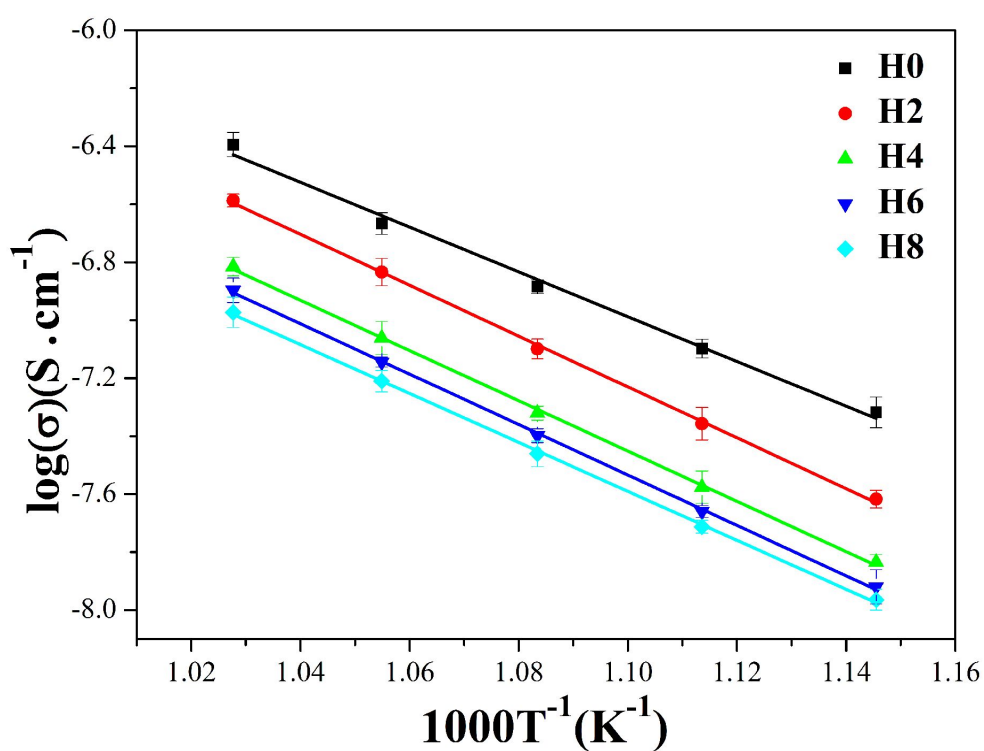


Fig.5 The temperature dependence of conductivity ($\log \sigma$ versus $1000 T^{-1}$), measured in air from 600 to 700 °C, for quenched glasses.

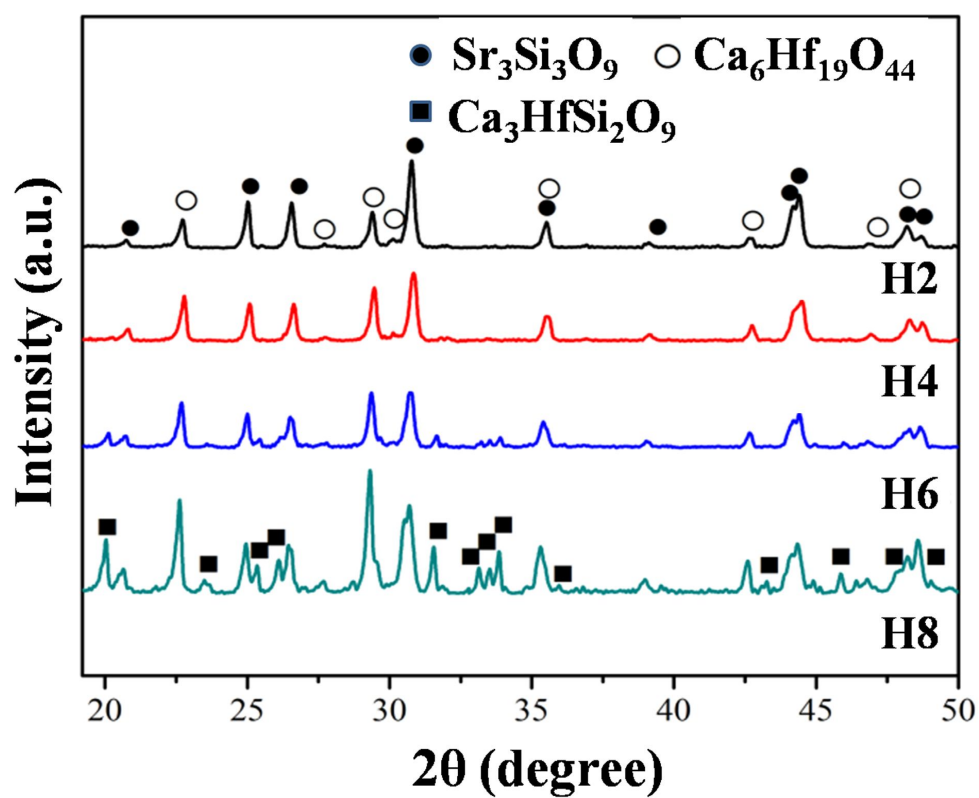


Fig.6 XRD patterns of glass-ceramics held at 800 °C for 100 hours.

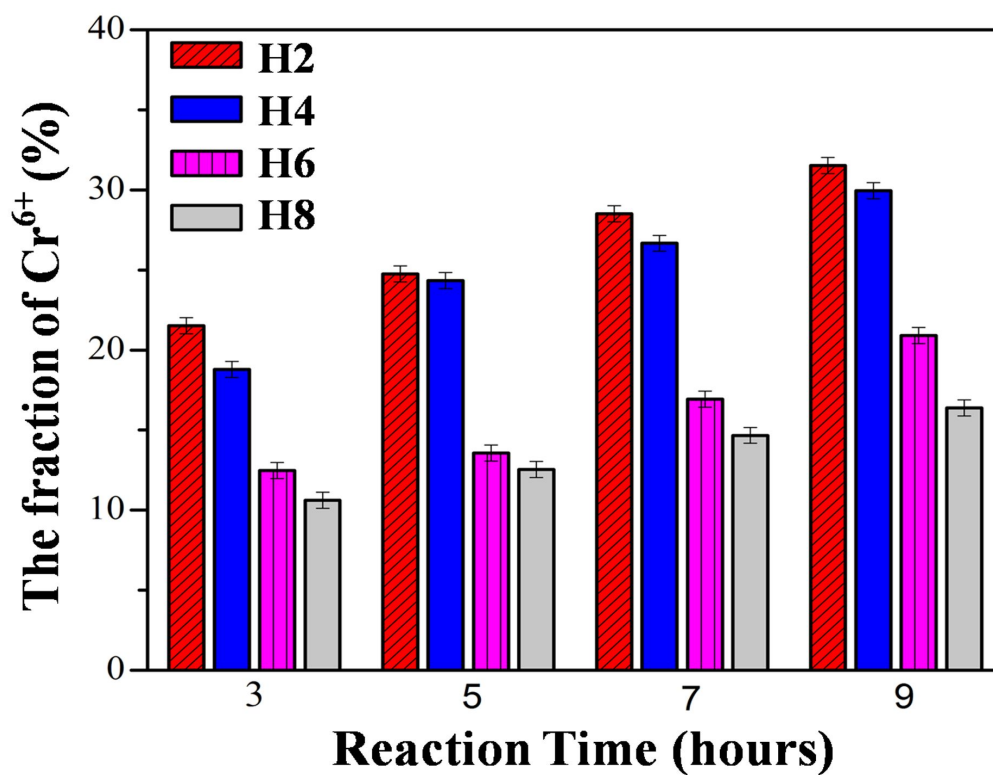
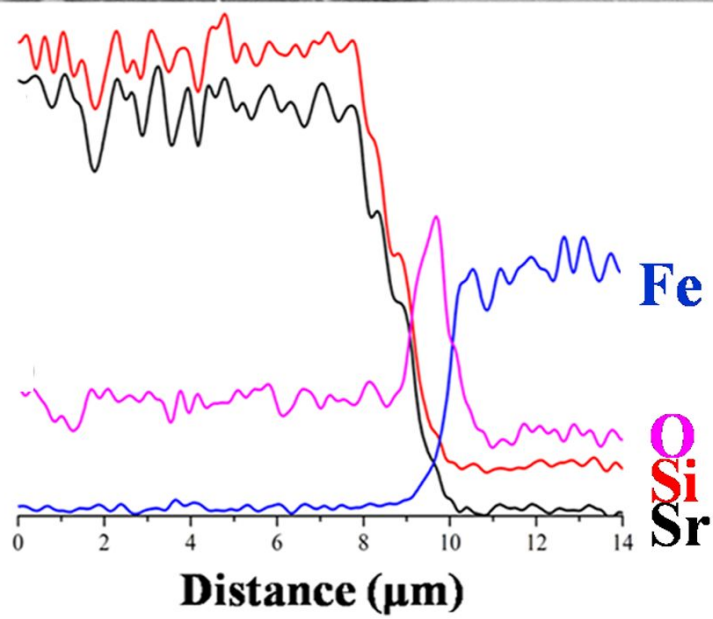
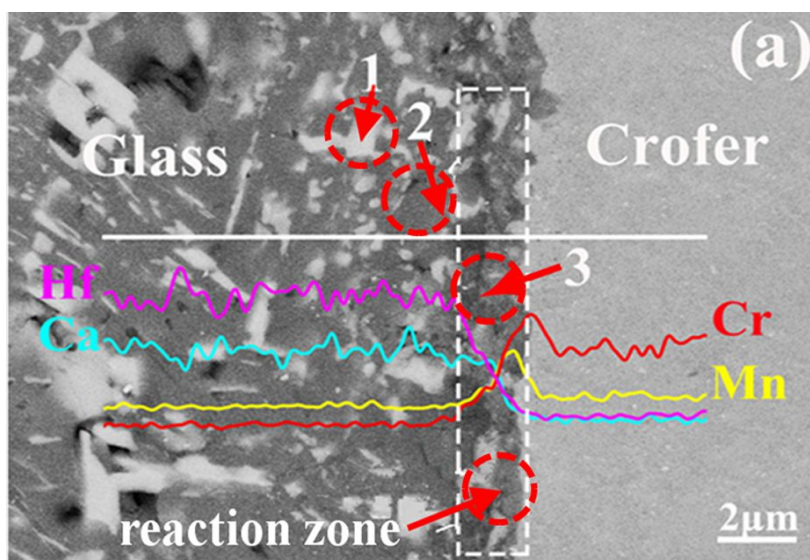


Fig.7 The fraction of Cr⁶⁺ in the reaction couples between Cr₂O₃ and glass powders, after reacting in air at 700 °C, as a function of reaction time.



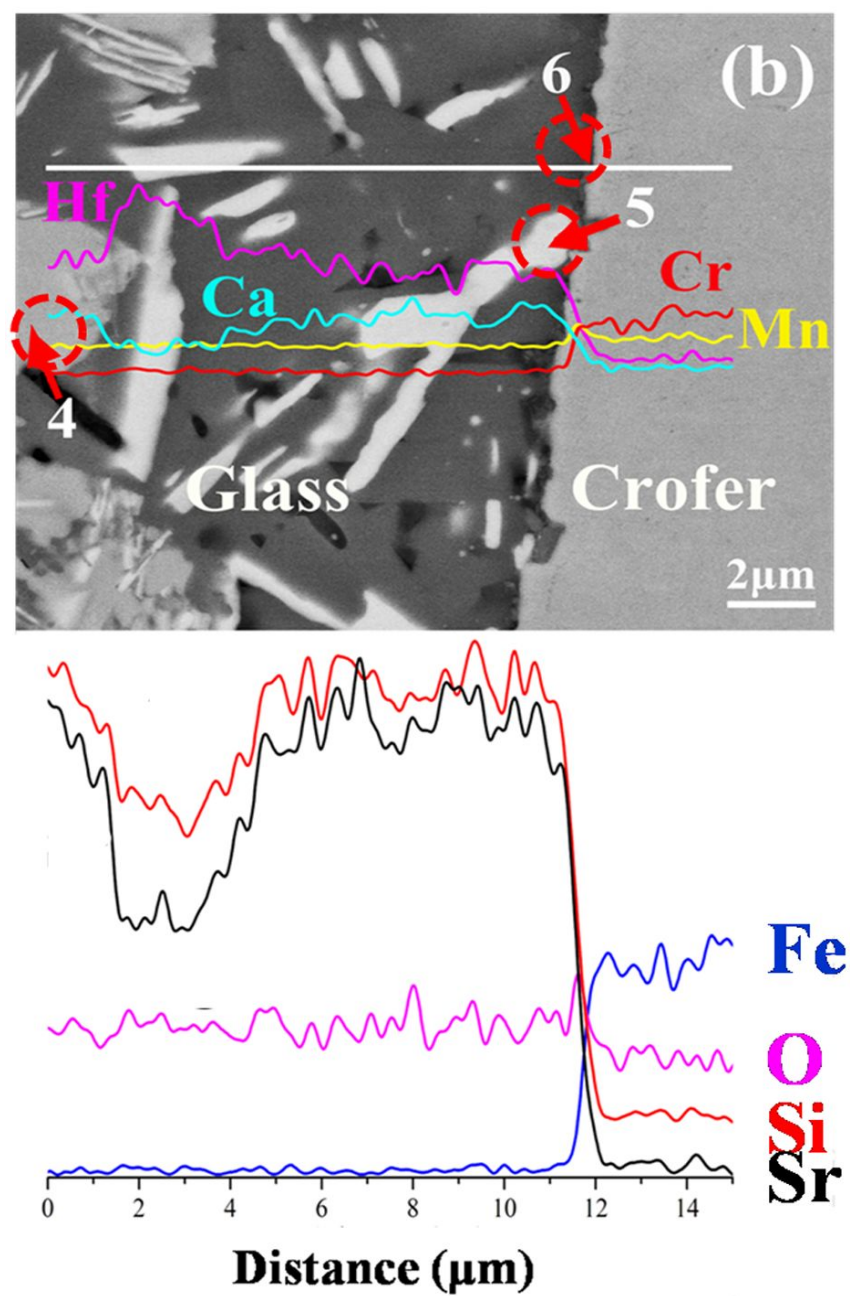
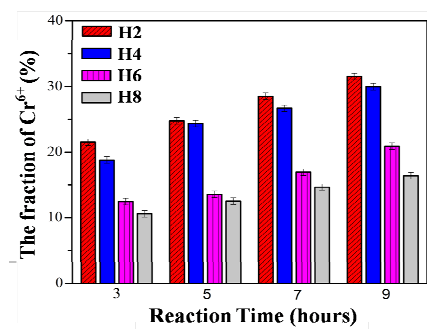


Fig.8 Micrographs of glass-ceramics/metal interfaces held at 800 °C for 100 hours, and EDS elemental line scans across the respective interfaces, for (a) glass containing 2 mol% HfO₂ and (b) glass containing 8 mol% HfO₂.



HfO₂ condenses the glass structure, blocks the interdiffusion between glasses and Cr-containing interconnects, and thus reduces the detrimental interfacial reaction.